

A 3D Simulation of a Neutrino-Driven Supernova Explosion Aided By Convection and Magnetic Fields

Bernhard Müller^{1,2}[★] and Vishnu Varma¹

¹*School of Physics and Astronomy, Monash University, VIC 3800, Australia*

²*ARC Centre of Excellence for Gravitational Wave Discovery – OzGrav*

11 August 2020

ABSTRACT

We study the impact of a small-scale dynamo in core-collapse supernovae using a 3D neutrino magnetohydrodynamics simulation of a $15M_{\odot}$ progenitor. The weak seed field is amplified exponentially in the gain region once neutrino-driven convection develops, and remains dominated by small-scale structures. About 250 ms after bounce, the field energy in the gain region reaches $\sim 50\%$ of kinetic equipartition. This supports the development of a neutrino-driven explosion with modest global anisotropy, which does not occur in a corresponding model without magnetic fields. Our results suggest that magnetic fields may play a beneficial subsidiary role in neutrino-driven supernovae even without rapid progenitor rotation. Further investigation into the nature of magnetohydrodynamic turbulence in the supernova core is required.

Key words: supernovae: general — turbulence — MHD

1 INTRODUCTION

Magnetic field effects pervade many astrophysical fluid dynamics problems such as stellar surface convection, stellar winds, and star formation. It has long been speculated that magnetic fields also play a critical role in some core-collapse supernova explosions of massive stars. The idea of tapping the rotational energy stored in the supernova core using strong magnetic fields has a long history (e.g., Meier et al. 1976; Bisnovatyi-Kogan et al. 1976; Akiyama et al. 2003; Burrows et al. 2007). In recent years models of such magnetorotational explosions have matured considerably, and three-dimensional (3D) simulations based on rapidly rotating stellar progenitor models are now available (Winteler et al. 2012; Mösta et al. 2014; Obergaulinger & Aloy 2017; Kuroda et al. 2020). Since strong magnetic fields in the progenitor star would lead to effective core spin-down, magnetorotational explosions require some amplification mechanism to generate strong large-scale magnetic fields on short time scales after core collapse, such as the magnetorotational instability (Balbus & Hawley 1991; Akiyama et al. 2003) or an α - Ω dynamo in the proto-neutron star (PNS) convection zone (Raynaud et al. 2020). Despite progress in understanding these amplification processes by means of idealized local and global simulations and analytic theory (Obergaulinger et al. 2009; Masada et al. 2012; Sawai et al. 2013; Guilet et al. 2015; Mösta et al. 2015; Raynaud et al. 2020; Masada et al. 2020), the stellar pre-collapse rotation rate remains a

major unknown for this supernova mechanism. Current stellar evolution models including magnetic torques (Heger et al. 2005) predict core spin rates that are too low for magnetorotational explosions, and still underestimate core spin-down in the case of low-mass red giants (Cantiello et al. 2014) for which asteroseismic measurements are available. Thus, magnetorotational explosions are likely rare and probably only explain “hypernovae” with unusually high explosion energies. For the majority of massive stars with moderate or slow core rotation, the neutrino-driven mechanism (Müller 2016) remains the favored scenario.

Magnetohydrodynamic (MHD) effects in non-rotating or slowly-rotating progenitors have received less attention, though a few studies have explored the amplification and dynamical role of Alfvén waves (Suzuki et al. 2008; Guilet et al. 2011) and field amplification by the standing accretion shock instability (Endeve et al. 2010, 2012). Supernova simulations of non-rotating progenitors with MHD and neutrino transport have so far been conducted in axisymmetry (2D) only (Obergaulinger et al. 2014). These models have indicated that for strong fields of $\sim 10^{12}$ G, MHD effects could play an auxiliary role in neutrino-driven explosions by facilitating the formation of large high-entropy bubbles.

However, MHD effects could play a more important and more generic role in neutrino-driven supernovae than these 2D simulations suggested, since dynamo field amplification cannot operate in 2D (Cowling 1933). More efficient field amplification might occur in 3D by a small-scale turbulent dynamo. A small-scale dynamo was in fact seen in idealized 3D simulations of the standing accretion shock instability by

[★] E-mail: bernhard.mueller@monash.edu

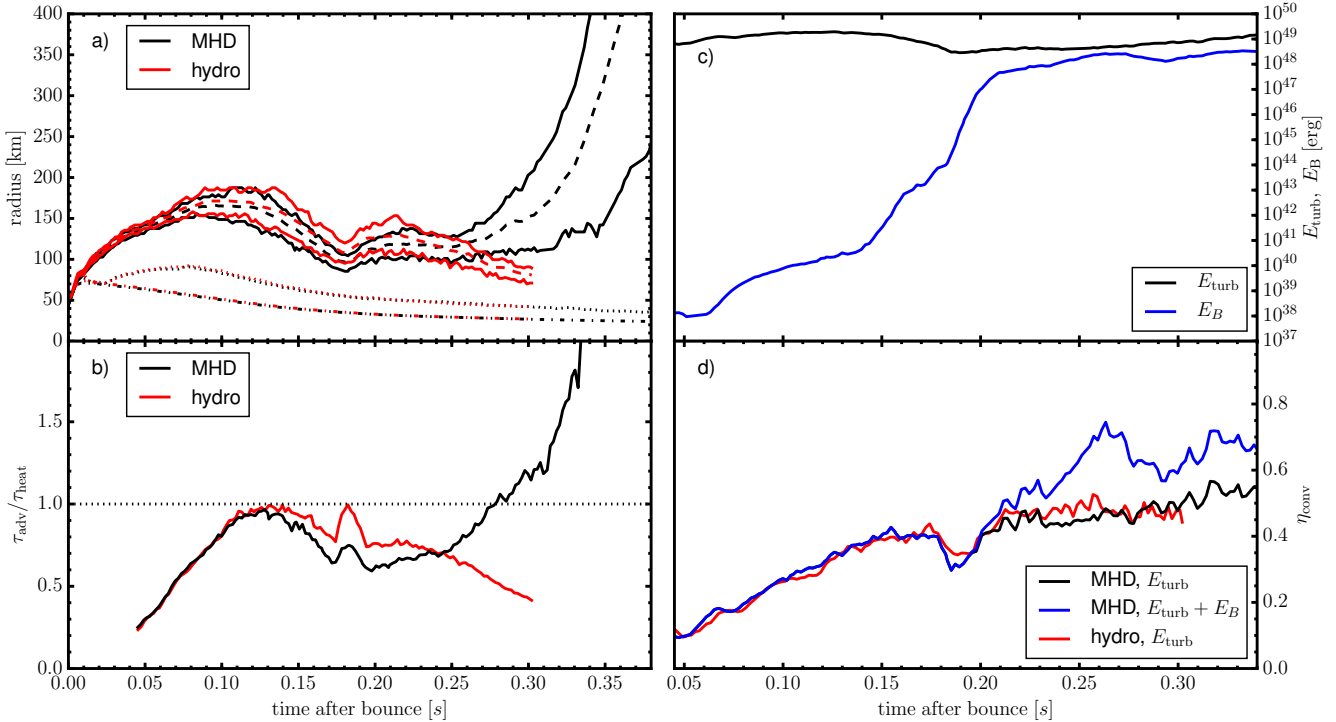


Figure 1. Evolution of the MHD model (black/blue curves) and the hydro model (red). a) Maximum, minimum (solid) and average shock radius (dashed), gain radius (dotted), and proto-neutron star radius (dash-dotted). b) Critical time scale ratio $\tau_{\text{adv}}/\tau_{\text{heat}}$. c) Turbulent kinetic energy E_{turb} (black) and magnetic energy in the gain region (blue) in the MHD model. d) Efficiency η_{conv} for the conversion of neutrino heating into turbulent energy kinetic energy (black/red) or total turbulent energy including magnetic fields (blue).

Endeve et al. (2012), though the fields did not become dynamically significant in their study. Moreover, conventional estimates for the field strengths in the cores and inner shells of massive stars could be too pessimistic. The magnetic field strengths of 10^3 – 10^9 G in white dwarfs (Ferrario et al. 2015) may not be indicative of the conditions in massive stars at the pre-collapse stage, where convective burning could generate strong small-scale fields via a turbulent dynamo. Considering ubiquitous observations of magnetic field strengths close to kinetic equipartition in similar settings (Christensen et al. 2009; Brun & Browning 2017), one should expect fields of order 10^{10} – 10^{11} G in the innermost active burning shells at collapse. Here we explore the amplification of such seed fields by a small-scale dynamo and their interplay with neutrino heating and the hydrodynamic instabilities in a progenitor with a moderate rotation rate for the first time in a 3D MHD simulation with neutrino transport.

2 PROGENITOR MODEL AND INITIAL CONDITIONS

We simulate the collapse of the $15M_{\odot}$ model m15b6 from Heger et al. (2005), whose evolution up to collapse has been calculated assuming magnetic torques. The progenitor has a central rotation rate of 0.05 rad s^{-1} , which translates into a neutron star birth spin period of 11 ms assuming that the collapsing core does not exchange angular momentum with the ejecta during the explosion. The neutron star’s rotational

energy of $\sim 2 \times 10^{50}$ erg would thus be too small to power a supernova with normal energy by MHD effects alone.

We perform two simulations with and without magnetic fields. Following Obergaulinger & Aloy (2017), we assume a dipolar field geometry given by the vector potential,

$$(A_r, A_{\theta}, A_{\varphi}) = (rB_{t,0}(r) \cos \theta, 0, r/2 \times B_{p,0}(r) \sin \theta), \quad (1)$$

in terms of the radius-dependent poloidal and toroidal field strengths $B_{p,0}$ and $B_{t,0}$. Realistic seed fields are likely dominated by smaller scales, but in default of better pre-collapse models, the assumption of a dipolar geometry appears justified as our findings do not appear to hinge on the large-scale structure of the field. In order not to overestimate the impact of magnetic fields, we reduce the poloidal and toroidal field strengths $B_{p,\text{prog}}$ and $B_{t,\text{prog}}$ in the progenitor by a factor of 10^4 , i.e., $B_{p,0} = 10^{-4} B_{p,\text{prog}}$ and $B_{t,0} = 10^{-4} B_{t,\text{prog}}$. In the progenitor, $B_{p,\text{prog}}$ and $B_{t,\text{prog}}$ reach values of 5×10^9 G and 10^6 G in non-convective regions as predicted by the Tayler-Spruit dynamo (Spruit 2002). Inside convective regions one expects values of $B_{p,\text{prog}}$ and $B_{t,\text{prog}}$ close to kinetic equipartition, which translates into a plasma beta (defined as the ratio of thermal to magnetic pressure) of $\beta = 10^4$ for the typical convective Mach numbers of $\sim 10^{-2}$ in the innermost burning shells at collapse (Collins et al. 2018). This would imply rather strong fields of up to 3×10^{12} G inside a small central region of radius 40 km and 6×10^{10} G in the oxygen shell, but after rescaling by a factor 10^{-4} , the seed fields can clearly not play any dynamical role after collapse without dynamo field amplification.

3 NUMERICAL METHODS

The simulations have been conducted with the Newtonian version of the CoCoNuT-FMT code (Müller & Janka 2015) using an effective gravitational potential (Case Arot) from Müller et al. (2008). The code has been updated to solve the Newtonian MHD equations using the extended HLLC solver of Gurski (2004); Miyoshi & Kusano (2005) and an energy-conserving variant of hyperbolic divergence cleaning (Dedner et al. 2002) following ideas from Tricco et al. (2016). Excluding terms for neutrino interactions and nuclear reactions, the extended system of MHD equations for the density ρ , velocity \mathbf{v} , magnetic field \mathbf{B} , total energy density e , and the Lagrange multiplier $\hat{\psi}$ reads,

$$\partial_t \rho + \nabla \cdot \rho \mathbf{v} = 0, \quad (2)$$

$$\partial_t (\rho \mathbf{v}) + \nabla \cdot \left(\rho \mathbf{v} \mathbf{v} - \frac{\mathbf{B} \mathbf{B}}{4\pi} + P_t \mathcal{I} \right) = \rho \mathbf{g} - \frac{(\nabla \cdot \mathbf{B}) \mathbf{B}}{4\pi}, \quad (3)$$

$$\partial_t e + \nabla \cdot \left[(e + P_t) \mathbf{v} - \frac{\mathbf{B}(\mathbf{v} \cdot \mathbf{B})}{4\pi} \right] = \rho \mathbf{g} \cdot \mathbf{v}, \quad (4)$$

$$\partial_t \mathbf{B} + \nabla \cdot (\mathbf{v} \mathbf{B} - \mathbf{B} \mathbf{v}) + \nabla \cdot (c_h \hat{\psi}) = 0 \quad (5)$$

$$\partial_t \hat{\psi} + c_h \nabla \cdot \mathbf{B} = -\hat{\psi} / \tau. \quad (6)$$

where \mathbf{g} is the gravitational acceleration, P_t is the total pressure, \mathcal{I} is the Kronecker tensor, c_h is the cleaning speed, and τ is the damping time scale for divergence cleaning. Note that the total energy density $e = \rho(\epsilon + v^2/2) + (B^2 + \hat{\psi}^2)/(8\pi)$ includes a contribution from $\hat{\psi}$ in addition to the internal energy ϵ , the kinetic energy, and the magnetic energy. To reduce numerical dissipation near the grid axis in our simulations, we have modified the mesh coarsening algorithm of Müller et al. (2019) by implementing a third-order accurate slope-limited prolongation scheme. Further details on the MHD implementation will be presented in a code comparison paper (Varma et al., in preparation). The equations for the electron fraction and mass fractions are the same as in the hydrodynamic case (Müller 2020). Neutrinos are treated using the FMT (fast multi-group transport) scheme of Müller & Janka (2015), which solves the energy-dependent zeroth moment equation for three neutrino species in the stationary approximation using a closure obtained from a two-stream solution of the Boltzmann equation (for details such as the neutrino rates, see Müller & Janka 2015). The models are run with a grid resolution of $550 \times 128 \times 256$ zones in radius, latitude, and longitude (corresponding to 1.4° in angle) with a non-equidistant grid in radius out to 10^5 km, and an exponential grid in energy space with 21 zones from 4 MeV to 240 MeV. We use the equation of state of Lattimer & Swesty (1991) with a bulk incompressibility of $K = 220$ MeV in the high-density regime, and the same low-density treatment as in previous CoCoNuT-FMT simulations (e.g., Müller & Janka 2015).

4 SIMULATION RESULTS

The maximum, minimum, and average shock radii evolve very similarly in the MHD model and the hydro model up to 250 ms after bounce (Fig. 1a). Small differences arise because of stochastic variations during prompt convection, which affect the entropy profiles of the PNS mantle and translate into a slightly smaller PNS radius and gain radius in the MHD

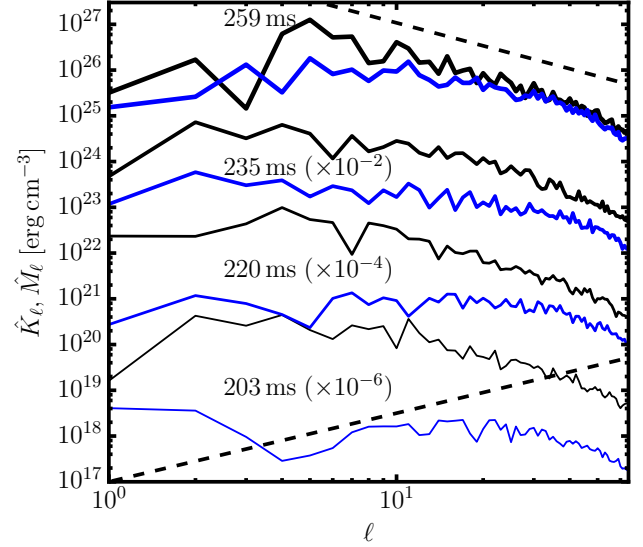


Figure 2. Angular power spectra \hat{K}_ℓ and \hat{M}_ℓ of the energy contained in radial turbulent motions (black) and the radial component of the magnetic field (blue) for the MHD model at different post-bounce times, measured in the lower half of the gain region. Dashed lines indicate slopes of $-5/3$ and $3/2$ for Kolmogorov and Kazantsev spectra.

model. These differences are also reflected in the critical ratio between the advection time scale τ_{adv} and the heating time scale τ_{heat} that quantifies the proximity to runaway shock expansion (Buras et al. 2006); $\tau_{\text{adv}}/\tau_{\text{heat}}$ is initially smaller in the MHD model.

Around 250 ms, however, the critical ratio $\tau_{\text{adv}}/\tau_{\text{heat}}$ and the shock radius in the MHD model overtake the hydro model. At 275 ms the runaway condition $\tau_{\text{adv}}/\tau_{\text{heat}} > 1$ is met, and steady shock expansion commences with the maximum shock radius reaching 1160 km by the end of the simulation. The diagnostic explosion energy (Buras et al. 2006) has only reached 2.3×10^{49} erg at this stage, but is growing at a rate of 4×10^{50} erg s^{-1} . No explosion develops in the hydro simulation in agreement with results obtained with more sophisticated neutrino transport for the same progenitor (Summa et al. 2018).

The trend towards better heating conditions and shock expansion in the MHD simulation sets in as soon as the magnetic fields in the gain region are amplified close to equipartition with the turbulent kinetic energy. This is illustrated by Fig. 1c, which shows the turbulent kinetic energy E_{turb} in the gain region, and the magnetic field energy E_B between the shock and the radius where the cooling rate per unit mass peaks. E_{turb} and E_B are computed as

$$E_{\text{turb}} = \int \frac{1}{2} \rho |\mathbf{v}'|^2 dV, \quad E_B = \int \frac{|\mathbf{B}'|^2}{8\pi} dV, \quad (7)$$

where \mathbf{v}' denotes the fluctuations of \mathbf{v} around its mass-weighted spherical average. Exponential field amplification starts once convection in the gain region develops and proceeds at a growth rate of the order of the inverse convective turnover time, which conforms to the expected behavior of a small-scale dynamo (Schober et al. 2012). The growth rate initially increases with time as the shock con-

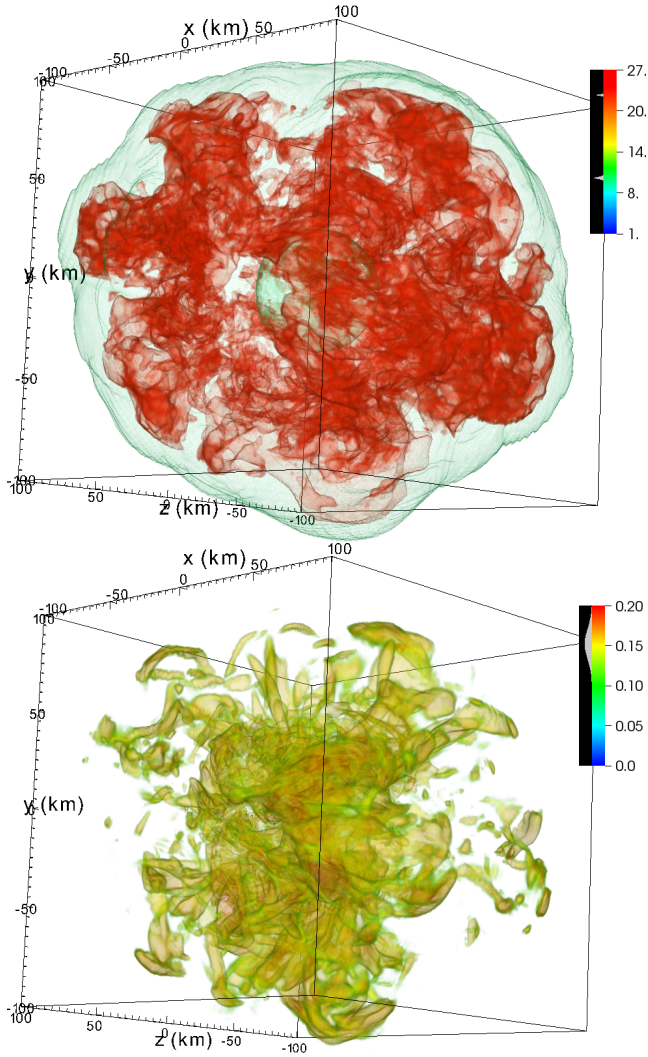


Figure 3. Volume rendering of the entropy in $k_B/\text{nucleon}$ (top) and the inverse of the plasma- β (bottom) for the MHD model at a time of 260ms. Neutrino-heated bubbles are visible in red and the shock and PNS surface in light green in the top panel. The magnetic field is dominated by small-scale structures. It is distributed relatively homogeneously across the gain region, though it tends to be expelled from bigger convective bubbles.

tracts and convection becomes increasingly violent. About 210ms, the growth of E_B slows down and is roughly linear as expected for a small-scale dynamo after kinetic equipartition is reached for the highest wave numbers (Cho et al. 2009). The ratio E_B/E_{turb} peaks at 50% around shock revival, i.e., at about the expected level in the relevant regime of high magnetic Prandtl number (Schober et al. 2015) that is relevant in the supernova core. The kinetic and magnetic energy spectra also exhibit the characteristic features of small-scale dynamo amplification. Fig. 2 shows angular power spectra \hat{K}_ℓ and \hat{M}_ℓ of the kinetic and magnetic energy contained in the radial components of the velocity field and magnetic

field,

$$\hat{K}_\ell = \frac{1}{2} \sum_{m=-\ell}^{\ell} \left| \int Y_{\ell m}^*(\theta, \varphi) \sqrt{\rho v_r} d\Omega \right|^2, \quad (8)$$

$$\hat{M}_\ell = \frac{1}{8\pi} \sum_{m=-\ell}^{\ell} \left| \int Y_{\ell m}^*(\theta, \varphi) B_r d\Omega \right|^2, \quad (9)$$

which we compute in the middle of the lower half of the gain region. During the exponential growth phase there is (leaving aside some jitter at low ℓ) initially a peak at high ℓ in \hat{M}_ℓ and a slightly positive spectral slope below, which is a little flatter than the expected Kazantsev spectrum with a power-law slope of $3/2$ (Brandenburg 2001; Brandenburg & Subramanian 2005), though the small spectral range does not permit a precise determination of the power-law slope. Once \hat{M}_ℓ approaches \hat{K}_ℓ at high wave numbers, the growth rate of the turbulent magnetic energy slows down and a Kolmogorov-like spectrum emerges, though \hat{M}_ℓ retains a shallower slope than \hat{K}_ℓ . While the dipole component is non-negligible, the spatial configuration of the field remains dominated by small-scale structures with little global anisotropy (Fig. 3)

Although the behaviour of the MHD model is compatible with the gross features of a small-scale dynamo, there are subtle differences to field amplification by isotropic and homogeneous turbulence. Amplification is driven mostly by shear motions around the gain radius, and the lowest values of the plasma- β are reached in this layer in line with the notion of flux expulsion from convective regions (Weiss 1966). However, the fields approach or even exceed equipartition with the thermal energy in strongly magnetized filaments (Fig. 3) whose volume fraction increases with time.

It remains to be discussed why magnetic field amplification close to kinetic equipartition results in more favorable conditions for shock revival. Supernova theory has established that the beneficial role of *hydrodynamic* “turbulence” (in the broad sense of deviations of the flow from spherical symmetry) is through Reynolds stresses and turbulent heat transfer between the gain radius and the shock, and that the size of these beneficial effects depends on the turbulent kinetic energy (Müller & Janka 2015; Müller 2020; Couch & Ott 2015). Similarly, beneficial effects of magnetic fields, e.g., an extra contribution of magnetic pressure and a reduction of the binding energy of the gain region, should scale with the magnetic energy. Although it is by no means clear that adding the same turbulent kinetic or magnetic energy has the same impact on the explosion conditions, it is therefore instructive to compare the total turbulent kinetic and magnetic energy in and immediately below the gain region in the MHD model and the hydro model. Since the turbulent motions are driven by neutrino heating, we consider the dimensionless efficiency parameter $\eta_{\text{conv}} = E_{\text{turb}}/(\dot{Q}_v \Delta R)^{2/3}$ (Müller & Janka 2015), where \dot{Q}_v is the volume-integrated heating rate in the gain region and ΔR is the width of the gain region. Fig. 1d shows that, when taking only the turbulent kinetic energy into account, η_{conv} is very similar in the magnetic and non-magnetic case, reaching a plateau at $\eta_{\text{conv}} \approx 0.5$ once convection has fully developed. If the magnetic energy is included, $\eta_{\text{conv}} = (E_{\text{turb}} + E_B)/(\dot{Q}_v \Delta R)^{2/3}$ reaches significantly higher values. In other words, a larger amount of total turbulent energy can be stored in the gain

region for the same neutrino heating rate if magnetic fields are present; it is not that the same amount of energy needs to be shared between turbulent motions and the additional degrees of freedom in the system. This is in line with the finding that the magnetic contributions to the turbulent energy flux in the gain region almost vanishes. Maintaining balance between neutrino heating and the turbulent energy flux in a quasi-steady state therefore requires similar convective velocities in the magnetic and non-magnetic case, and the turbulent magnetic energy will be added on top on a level set by the balance between field amplification and the backreaction of the fields on the flow.

5 CONCLUSIONS

Our simulations suggest that magnetic fields can have a substantial and beneficial impact on neutrino-driven shock revival even in slowly rotating progenitors with weak seed fields. Field amplification by a small-scale dynamo in the gain region is sufficient to amplify fields almost to kinetic equipartition within the first hundreds of milliseconds after bounce. Judging by the turbulent magnetic energy that can be reached, adding magnetic fields does, however, have a smaller impact than going from spherically symmetric models to multi-dimensional hydrodynamic models. The effect size of magnetic fields on the explosion conditions will need to be compared to other factors that influence the heating conditions, such as general relativity and the treatment of neutrino transport and neutrino interactions. Considering their impact on $\tau_{\text{adv}}/\tau_{\text{heat}}$, magnetic fields are likely one among many factors that can contribute to a similar degree to successful explosions in generic, slowly rotating supernova progenitors without qualitatively changing the picture of neutrino-driven explosions.

Our MHD simulation prompts a number of questions for future research. To avoid an overproduction of magnetars, one important constraint is that the neutron star magnetic fields created during a typical explosion must not be *too strong*. In our MHD model, the dipole field strength on a density isosurface at $\sim 10^{10} \text{ g cm}^{-3}$ is several 10^{13} G and hence somewhat on the high side for typical pulsars. However, the final dipole field strength of the neutron star cannot be confidently predicted from our short simulation. Turbulent reconnection and field burial (Torres-Forné et al. 2016) may yet bring the dipole field strength down to lower values. Nor can we exclude that the relatively strong dipole has arisen by chance, due to limitations in numerical resolution, or due to the choice of the initial field. Clearly, more simulations are needed to determine the robustness of our results; unfortunately the closest analog to our models – the idealized 3D simulations of Endeve et al. (2012) – are far too different in design to offer a meaningful point of comparison.

Further work is also required to investigate whether our results are sensitive to non-ideal effects. Conservative estimates of the physical viscosity and resistivity based on (Spitzer 1965) place the magnetic Prandtl number in the gain region on the order of $\text{Pm} > 10^3$. While our ideal MHD simulation comports with the expectations for $\text{Pm} > 1$, the numerical Prandtl number is likely no more than a few (Federrath et al. 2011). The numerical Reynolds number is also bound to be well below the physical value of $\text{Re} \sim 10^{15}$

(Abdikamalov et al. 2015). Since the growth rate of the small-scale dynamo for $\text{Pm} \gg 1$ scales with $\text{Re}^{1/2}$ during the kinematic phase (Schober et al. 2012), saturation on the resistive scale should be reached almost instantly in nature, but the question becomes whether the growth of the field on larger scales during the subsequent dynamic phase is slow and whether saturation may happen well below kinetic equipartition under certain conditions (Schekochihin et al. 2002). Simulations (Haugen et al. 2004) and more recent analytic models (e.g., Stepanov & Plunian 2008; Schober et al. 2015) do not support such adverse effects on the growth and saturation of the small-scale dynamo for $\text{Pr} > 1$. However, any extrapolation to the physical regime is still far from certain, and substantial neutrino drag (Melson et al. 2020) in the shear layer at the bottom of the gain region further complicates the picture. Much remains to be done to substantiate the interesting prospect that magnetic fields may play a beneficial subsidiary role in shock revival next to neutrino heating and hydrodynamical turbulence.

ACKNOWLEDGEMENTS

BM was supported by ARC Future Fellowship FT160100035. This research was undertaken with the assistance of resources and services from the National Computational Infrastructure (NCI) and the Pawsey Supercomputing Centre.

DATA AVAILABILITY

The data underlying this article will be shared on reasonable request to the corresponding author.

REFERENCES

- Abdikamalov E., et al., 2015, *ApJ*, 808, 70
- Akiyama S., Wheeler J. C., Meier D. L., Lichtenstadt I. Meier D. L., Lichtenstadt 2003, *ApJ*, 584, 954
- Balbus S. A., Hawley J. F., 1991, *ApJ*, 376, 214
- Bisnovatyi-Kogan G. S., Popov I. P., Samokhin A. A., 1976, *Ap&SS*, 41, 287
- Brandenburg A., 2001, *ApJ*, 550, 824
- Brandenburg A., Subramanian K., 2005, *Phys. Rep.*, 417, 1
- Brun A. S., Browning M. K., 2017, *Living Reviews in Solar Physics*, 14, 4
- Buras R., Janka H.-T., Rampp M., Kifonidis K., 2006, *A&A*, 457, 281
- Burrows A., Dessart L., Livne E., Ott C. D., Murphy J., 2007, *ApJ*, 664, 416
- Cantiello M., Mankovich C., Bildsten L., Christensen-Dalsgaard J., Paxton B., 2014, *ApJ*, 788, 93
- Cho J., Vishniac E. T., Beresnyak A., Lazarian A., Ryu D., 2009, *ApJ*, 693, 1449
- Christensen U. R., Holzwarth V., Reiners A., 2009, *Nature*, 457, 167
- Collins C., Müller B., Heger A., 2018, *MNRAS*, 473, 1695
- Couch S. M., Ott C. D., 2015, *ApJ*, 799, 5
- Cowling T. G., 1933, *MNRAS*, 94, 39
- Dedner A., Kemm F., Kröner D., Munz C. D., Schnitzer T., Wesenberg M., 2002, *Journal of Computational Physics*, 175, 645
- Endeve E., Cardall C. Y., Budiardja Mezzacappa A., 2010, *ApJ*, 713, 1219

- Endeve E., Cardall C. Y., Budiardja R. D., Beck S. W., Bejnood A., Toedte R. J., Mezzacappa A., Blondin J. M., 2012, *ApJ*, 751, 26
- Federrath C., Chabrier G., Schober J., Banerjee R., Klessen R. S., Schleicher D. R. G., 2011, *Phys. Rev. Lett.*, 107, 114504
- Ferrario L., de Martino D., Gänsicke B. T., 2015, *Space Sci. Rev.*, 191, 111
- Guilet J., Foglizzo T., Fromang S., 2011, *ApJ*, 729, 71
- Guilet J., Müller E., Janka H.-T., 2015, *MNRAS*, 447, 3992
- Gurski K. F., 2004, *SIAM Journal on Scientific Computing*, 25, 2165
- Haugen N. E., Brandenburg A., Dobler W., 2004, *Phys. Rev. E*, 70, 016308
- Heger A., Woosley S. E., Spruit H. C., 2005, *ApJ*, 626, 350
- Kuroda T., Arcones A., Takiwaki T., Kotake K., 2020, *ApJ*, 896, 102
- Lattimer J. M., Swesty F. D., 1991, *Nuclear Physics A*, 535, 331
- Masada Y., Takiwaki T., Kotake K., Sano T., 2012, *ApJ*, 759, 110
- Masada Y., Takiwaki T., Kotake K., 2020,
- Meier D. L., Epstein R. I., Arnett W. D., Schramm D. N., 1976, *ApJ*, 204, 869
- Melson T., Kresse D., Janka H.-T., 2020, *ApJ*, 891, 27
- Miyoshi T., Kusano K., 2005, *Journal of Computational Physics*, 208, 315
- Mösta P., et al., 2014, *ApJ*, 785, L29
- Mösta P., Ott C. D., Radice D., Roberts L. F., Schnetter E., Haas R., 2015, *Nature*, 528, 376
- Müller B., 2016, *Publ. Astron. Soc. Australia*, 33, e048
- Müller B., 2020, *Living Rev. Comput. Astrophys.*, 6, 3
- Müller B., Janka H.-T., 2015, *MNRAS*, 448, 2141
- Müller B., Dimmelmeier H., Müller E., 2008, *A&A*, 489, 301
- Müller B., et al., 2019, *MNRAS*, 484, 3307
- Obergaulinger M., Aloy M. Á., 2017, *MNRAS*, 469, L43
- Obergaulinger M., Cerdá-Durán P., Müller E., Aloy M. A., 2009, *A&A*, 498, 241
- Obergaulinger M., Janka H.-T., Aloy M. A., 2014, *MNRAS*, 445, 3169
- Raynaud R., Guilet J., Janka H.-T., Gastine T., 2020, *Science Advances*, 6, eaay2732
- Sawai H., Yamada S., Kotake K., Suzuki H., 2013, *ApJ*, 764, 10
- Schekochihin A. A., Cowley S. C., Hammett G. W., Maron J. L., McWilliams J. C., 2002, *New Journal of Physics*, 4, 84
- Schober J., Schleicher D., Federrath C., Klessen R., Banerjee R., 2012, *Phys. Rev. E*, 85, 026303
- Schober J., Schleicher D. R. G., Federrath C., Bovino S., Klessen R. S., 2015, *Phys. Rev. E*, 92, 023010
- Spitzer L., 1965, *Physics of fully ionized gases*. Interscience Publishers, New York
- Spruit H. C., 2002, *A&A*, 381, 923
- Stepanov R., Plunian F., 2008, *ApJ*, 680, 809
- Summa A., Janka H.-T., Melson T., Marek A., 2018, *ApJ*, 852, 28
- Suzuki T. K., Sumiyoshi K., Yamada S., 2008, *ApJ*, 678, 1200
- Torres-Forné A., Cerdá-Durán P., Pons J. A., Font J. A., 2016, *MNRAS*, 456, 3813
- Tricco T. S., Price D. J., Bate M. R., 2016, *Journal of Computational Physics*, 322, 326
- Weiss N. O., 1966, *Proceedings of the Royal Society of London Series A*, 293, 310
- Winteler C., Käppeli R., Perego A., Arcones A., Vasset N., Nishimura N., Liebendörfer M., Thielemann F.-K., 2012, *ApJ*, 750, L22